Structural evolution, crystallization behaviour and mid-infrared emission properties in Yb/Ho codoped oxyfluoride germanosilicate glass ceramics with varied Si/Ge ratio

Y. Tian, Q. Liu, F. E, R. Ye, S. Chen, J. Zhang, S. Xu

Structural evolution, crystallization behaviour and mid-infrared emission properties in Yb/Ho codoped oxyfluoride germanosilicate glass ceramics with varied Si/Ge ratio

Ying Tian[a], Qunhuo Liu[b], Fei E[c], Renguang Ye[a,d,*], Shuting Chen[a], Junjie Zhang[a], Shiqing Xu[a,*]

[a]*Institute of photoelectric materials and devices, China Jiliang University, Hangzhou 310018, PR China*

[b]*State Key Laboratory of Silicon Materials &, School of Materials Science and Engineering, Zhejiang University, Hangzhou, China*

[c]*School of Optical-Electrical and Computer Engineering, University of Shanghai for Science and Technology, Shanghai, 200093, PR China*

[d]*University Rennes, CNRS, ISCR (Institut des Sciences Chimiques de Rennes) – UMR 6226, F-35000 Rennes, France*

* Corresponding author.

E-mail address: yerenguang@163.com(Renguang Ye), sxucjlu@163.com(Shiqing Xu)

Abstract:

Changes in glass structure and crystallization behaviour from oxyfluoride silicate glass to oxyfluoride germanate glass were studied by modifying the ratio of Si/Ge in oxyfluoride germanosilicate glass ceramics, and transparent glass ceramic with low light scattering and efficient mid-infrared emissions were obtained. The $NaYF_4$ nanocrystals crystallization ability of oxyfluoride glass was decreased with the increase in Ge content, which can be attributed to the weakened oxide and fluoride phase separation in GeO_2-rich glass. Upconversion and down-conversion emission spectra together with Ho^{3+}: $^5I_6$ energy level fluorescent decay curves have been discussed for SiO_2-rich glass ceramics and GeO_2-rich glass ceramics, in which the fluoride crystallization induced the decrease of multi-phonon non-radiative decay rates plays the main role in the energy transfer processes. The influence of Si/Ge ratio on 2μm and 3μm fluorescent emissions in glasses and glass ceramics, and its link with glass network structural changes were discussed. The optimized Yb/Ho codoped oxyfluoride germanosilicate glass ceramic with low light scattering, high peak emission cross section($11.18\times10^{-21}cm^2$) and maximum gain coefficient ($1.387cm^{-1}$) at 2888 nm provides a potential application in the development of new 3μm laser devices based on transparent oxyfluoride glass ceramic materials.

1. Introduction

Mid-infrared laser has been gaining momentum in the recent years due to their appeal and potential applications in eye-safe laser radar, laser surgery, remote sensing and pump source for far-infrared lasers[1-3]. Among various rare earth ions (REs), Ho^{3+} is

an important active ion to achieve 2μm and 3μm emission by its $^5I_7 \rightarrow {}^5I_8$ and $^5I_6 \rightarrow {}^5I_7$ transitions, respectively[4]. Codoping proper sensitized ions is the most efficient way to address the problem that Ho^{3+} has no suitable pump bands overlap with commercially available laser diode. Yb^{3+} ion is an efficient sensitizer, which can strongly absorb the pump light of 980 nm laser diode and subsequently transfer the energy to Ho^{3+} ion[5, 6].

Also important is to select an appropriate host material. It should consider a host material in aspects including preparation technologies, optical properties, mechanical properties, chemical properties and thermal properties[7-10]. Transparent oxyfluoride glass ceramics are novel and promising host materials, which have advantages of glasses and single crystals. They maintain the merits of glasses that can accommodate large amount of dopants and have a good applicability in size and shape such as fabricating fibers[11-13]. Compared with glasses, REs in glass ceramics are located at a lower phonon energy and more ordered environment provided by embedded fluoride nanocrystals (NCs), although not all REs are allocated in fluoride NCs[14]. Importantly, this means that the multi-phonon relaxation rate of doped REs would be reduced effectively, and thus a high efficient luminescence can be obtained. Owing to attractive merits mentioned above, transparent oxyfluoride glass ceramics have captured much attention of researchers and many types of glass ceramics have been developed. According to their chemical composition, they can be classified into silicate, germanate, phosphate, borate, tellurite and mixed type[14, 15].

Silicate and germanate glasses are generally considered to have a similar continuous three-dimensional network that is mainly made of SiO_4 or GeO_4 tetrahedra[16, 17]. However, when introducing fluoride into them, there are obvious differences between oxyfluoride silicate glass and oxyfluoride germanate glass in crystallization behaviour and luminescent properties. For instance, $NaLnF_4$ NCs with low phonon energy are readily precipitated in oxyfluoride silicate glasses[4, 18], but there is not yet any report on oxyfluoride germanate glass ceramic containing $NaLnF_4$ NCs. It is significant to understand why varied crystallization behaviour occur in these two conventional and important glasses, and investigation on a series of glasses changing with the content of SiO_2 and GeO_2 may help reveal the potential reasons. There have been many reports on the crystallization behaviour of fluorosilicate glass system[19-23]. The influence of glass composition, melting technique and heat-treatment condition on the $NaYF_4$ crystallization behaviour in fluorosilicate glass have been widely discussed experimentally and theoretically. Most of these studies show that the fluoride phase separation in fluorosilicate glass has a significant effect on the crystallization behaviour, which will lead to the increase of effective nucleation density of subsequent crystallization. And the composition and microstructure of fluoride phase determines the types of crystalline phase that are capable of precipitating from the glass during the heat-treatment process.

In this work, we investigated the crystallization behaviour, network structure and mid-infrared luminescent properties of the optimized oxyfluoride glass system SiO_2-GeO_2-Al_2O_3-Na_2O-NaF-YF_3-(YbF_3-HoF_3), with systematic variation of the silicate/germanate (Si/Ge) ratio. The crystallization behaviour of $NaYF_4$ NCs and structural evolution in glass ceramics have been investigated by their morphological

characteristics and vibrational spectra. The Judd-Ofelt (J–O) parameters were calculated to analyze the change of the ligand environment of Ho^{3+} ions based on measured absorption spectra and J–O theory. Spectroscopic properties including 2μm and 3μm fluorescent emission spectra, calculated absorption and emission cross sections and gain coefficient spectra have been studied to build structure-luminescence relationship and evaluate prepared glass ceramics potential as 3μm laser materials.

2. Experimental procedure

2.1 Samples preparation

Germanosilicate oxyfluoride glasses with varied Si/Ge ratio were prepared by the conventional high-temperature melt-quenching technique. In designing the compositional series selected, we have chosen to keep the relative content of different network-modifiers and intermediates constant, while varying the ratio of different network-formers by substitution of GeO_2 for SiO_2. The concrete molar composition was $(55\text{-}x)SiO_2\text{-}xGeO_2\text{-}10Al_2O_3\text{-}15Na_2O\text{-}10NaF\text{-}(10\text{-}3y)YF_3\text{-}2yYbF_3\text{-}yHoF_3$, where x=5, 15, 25, 35, 45 and 0, y=0 and 0.5. Glasses and glass ceramics without Yb/Ho doping (labeled as G1 to G6 and GC1 to GC6, respectively) were used in the study of crystallization behaviour and network structure, while Yb/Ho codoped glasses and glass ceramics (labeled as GH1 to GH6 and GCH1 to GCH6, respectively) were prepared to investigate the mid-infrared luminescent properties. The analytical grade raw materials with required proportion were thoroughly mixed and melted at 1450°C for 30min in a covered alumina crucible under normal atmosphere. The melts were subsequently quenched by pouring on a preheated stainsteel mold. Then the glasses were annealed at 450°C for 4h to remove the internal stress. In order to obtain transparent oxyfluoride glass ceramics, the precursor glasses were heat-treated for certain time. In order to compare the effects of components and treatment time on the properties of glass more conveniently, the treatment temperature is marked after the components of samples obtained at different heat treatment temperatures, such as Si50Ge5 575 ℃, which is the sample of Si50Ge5(contain mainly 50mol% SiO_2, 5mol% GeO_2 and other components) heat-treated at 575 ℃ for 3 h; Si50Ge5 635, which is the sample of Si50Ge5 heat-treated at 635 ℃ for 3 h. Finally, glass and glass ceramic samples were cut and polished into glass samples with thickness of 1 mm for structural and spectroscopic measurements.

2.2 Characterization

The densities of glass samples were measured according to the Archimedes principle using distilled water as the immersion liquid. X-ray diffraction (XRD) analysis of powder samples was measured by Rigaku D/max2550 diffractometer using Cu-Kα1 radiation. The micrographs of glass ceramic were performed with transmission electron microscope (TEM, FEI TF20). Fourier transformed infrared (FTIR) spectral measurements were performed in a Thermo Fisher Scientific. Raman spectra were measured by a Raman spectrometer from Renishaw (inVia, UK) excited by 532nm laser. Absorption spectra were carried out on a PerkinElmer Lambda 900UV−vis−NIR spectrophotometer with a resolution of 1 nm. Visible and

Near-infrared emission spectra were recorded using a FLS920 spectrometer from Edinburgh Instruments Ltd. Mid-infrared emission spectra were recorded using a FLS980 spectrometer from Edinburgh Instruments Ltd. and detected with a liquid-nitrogen-cooled PbS detector upon excitation by 980 nm LD. All the measures were taken at room temperature and other conditions were kept as same as possible.

3. Results and discussion

3.1 Glass structure and crystallization behaviour

Figure 1(a) shows the DTA curves of G1, G2, G3 and G4 sample, in which the characteristic temperatures could be determined, providing simple guidance for the control of nano-crystallization in oxyfluoride glasses. The beginning and peak of exothermic peak are generally considered as the onset crystallization temperature and the crystallization peak temperature, respectively. However, it was found that the crystallization behavior in SiO_2-rich glass occurs in the 575°C which is far below the so-called onset crystallization temperature as shown in Fig. 3(b). Similar phenomenon was observed in other glass system without explanation. With the heat-treatment temperature increasing to 635°C, the diffraction peak in XRD pattern of SiO_2-rich glass is stronger, while that of GeO_2-rich glass still not shows up. Besides, we observed the Si50Ge5 635 sample presents translucence (Fig. 1(c)) and high mechanical strength, while the Si0Ge55 635 sample become softened and deformed with relatively high transparency (Fig. 1(d)). With the heat-treatment temperature further increasing to 700°C, the Si50Ge5 700 sample maintain single $NaYF_4$ nanocrystalline phase and lower transparency, while the whole Si0Ge55 700 sample presents milk white and contains unknown crystals (Fig. 2(d)). The above crystallization behaviour indicate that the crystallization of fluoride component occurs while the residual oxide component maintains amorphous, which enables the Si50Ge5 635 sample with high mechanical strength and the growth of $NaYF_4$ nanocrystals reduces the transparency of glass ceramic. In comparison, the fluoride component won't be precipitated before the oxide component when the GeO_2-rich glass is heating. Therefore, the fluoride and oxide phase separation easily occur in SiO_2-rich glass but is greatly reduced in GeO_2-rich glass. The phase separation in the SiO_2-rich glass enables highly effective nucleation density and facilitates subsequent crystallization with low activation energy. The strong exothermic peak in Fig. 1a may be mainly caused by the combination and growth of small separated crystal phase. In GeO_2-rich glass, lack of phase-separation, the volume crystallization of the whole glass requires higher heat-treatment temperature with high activation energy. Fig. 1(b) shows the FTIR transmittance spectra of G1 and G6 powder sample, the OH^- content of two glasses is similar.

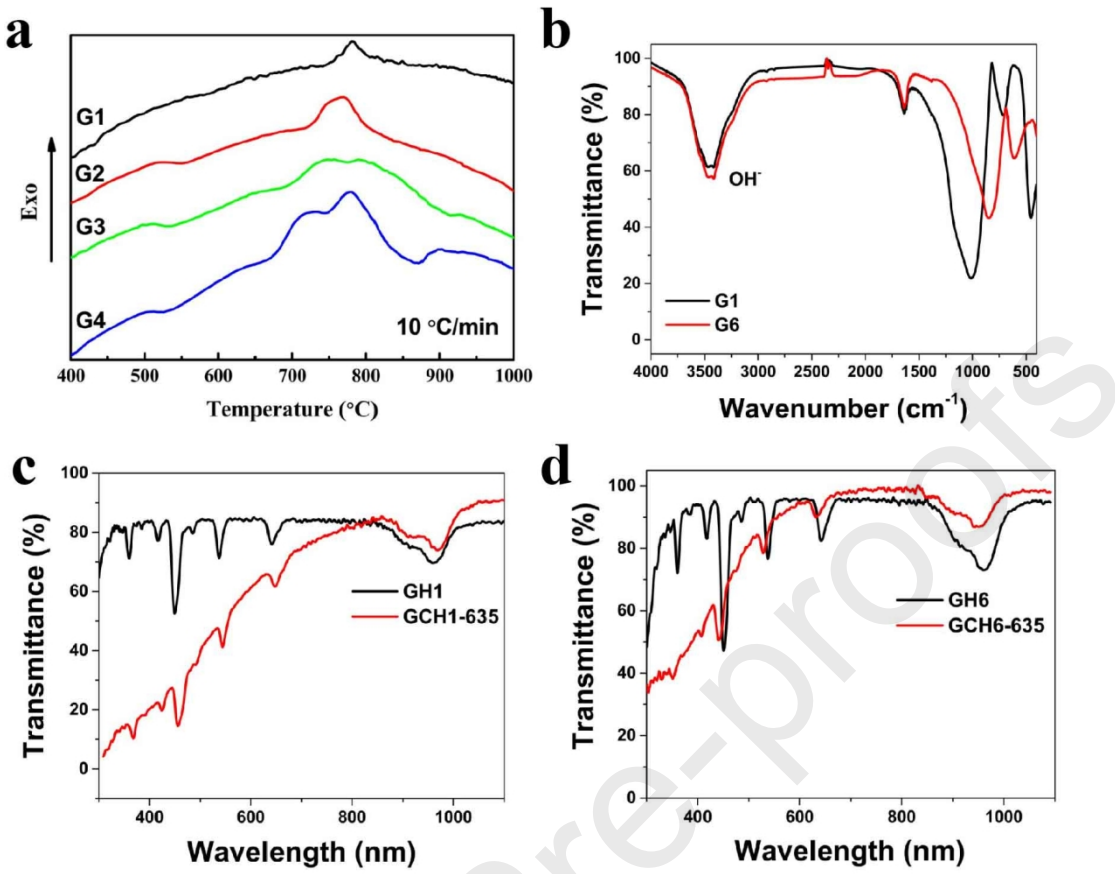

Fig. 1 (a) DTA curve of G1, G2, G3 and G4 glasses; (b) FTIR transmittance spectra of G1 and G6 powders; Transmittance spectra of GH1 and GCH1-635 (c) as well as GH6 and GCH6-635 (d) samples.

Figure 2(a) and (b) show two different regions in the Si50Ge5 635 sample, in which the nanocrystals of uneven size present a big difference, indicating the combination and growth of nanocrystals at such a temperature. Fortunately, High-resolution TEM (HRTEM) image of Si50Ge5 635 sample in Fig. 2(c), the lattice fringes display interplanar spacings of 0.296 and 0.207 nm in the particle, which match well with the (110) and (201) planes of the $NaYbF_4$ nanocrystals, indicating Yb^{3+} has enter into $NaYF_4$ nanocrystals, while the XRD results cannot provide such a direct evidence because of low content of Yb^{3+} ions in glass.

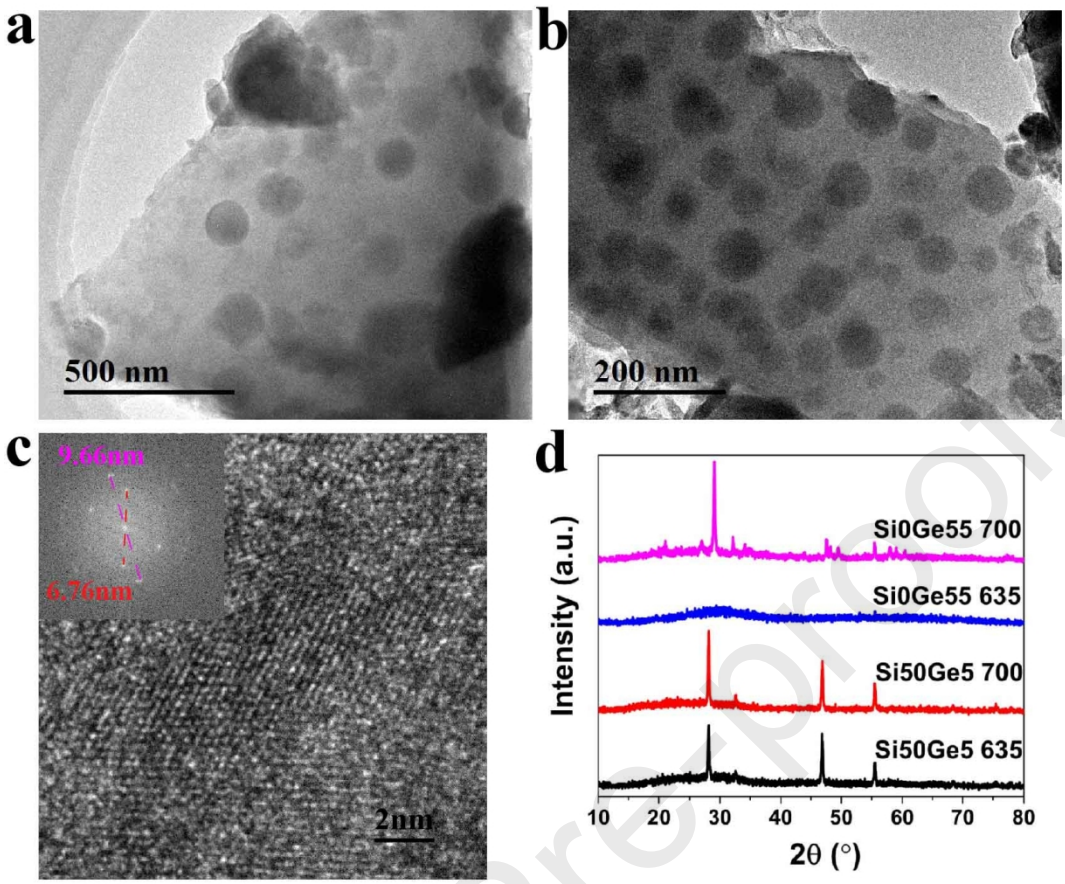

Fig.2 (a,b) TEM images of two regions in the Si50Ge5 635 sample; (c) HRTEM of the NaYF4 nanocrystals distributed in the Si50Ge5 635 sample, the inset is the FFT of HRTEM; (d) XRD patterns of Si50Ge5 and Si0Ge55 glass ceramics under two high heat-treatment temperature 635°C and 700°C

The XRD patterns of oxyfluoride glasses with different Si/Ge ratio were presented in Fig.3(a), and no diffraction peaks were observed for all glass samples, which indicated that the Si/Ge ratio has no obvious effect on the amorphous structure of glass and the oxyfluoride germanosilicate glass system has a widely adjustable glass former composition. Fig.3(b) shows the XRD patterns of oxyfluoride glass ceramics with different Si/Ge ratio, where five diffraction peaks were observed and they were well matched with standard card of $NaYF_4$ crystals (JCPDS No. 06-0342). The intensity of diffraction peaks gradually decreased with increasing Ge content and the diffraction peak was finally unobservable in GC6 sample. It indicated that the crystallization ability and number of $NaYF_4$ NCs in oxyfluoride glass were decreased when the Ge content was improved. Therefore, the GC6 host glass was removed in the following investigations of absorption and mid-infrared emission properties due to no $NaYF_4$ NCs crystallization in it.

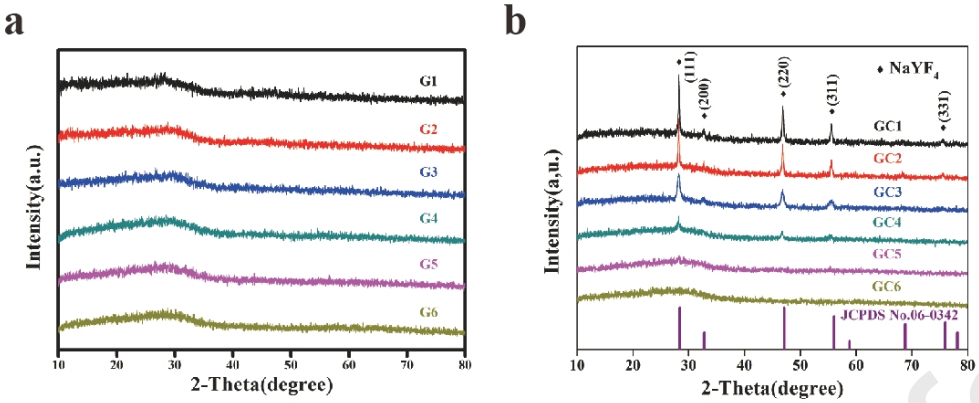

Fig.3 XRD patterns of oxyfluoride glasses (a) and glass ceramics (b) with different Si/Ge ratio

In order to investigate the variation of glass structure of oxyfluoride germanosilicate glasses and glass ceramics changing with Ge content, FTIR spectral analysis were performed to analyze the variation of relevant vibration peaks and microstructure evolution in glass network. In the FTIR spectra of oxyfluoride glass ceramics with different Si/Ge ratio(see Fig.4(a)), the band at around 1010 cm^{-1} was caused by Si-O-Si asymmetric stretching vibration, while the primary band at around 850 cm^{-1} was assigned to Ge-O-Ge asymmetric stretching vibration[17, 24]. Obviously, the former was decreased and the latter was increased, which can be easily attributed to the transformation between Si-O-Si, Si-O-Ge and Ge-O-Ge with Si/Ge ratio dropping. The lower Si-O bond strength and higher Ge-O bond strength can also result in similar change between Si-O-Si(Al) bending vibration at around 710 cm^{-1} and Ge-O-Ge(Al) bending vibration at around 600 cm^{-1}. The band at around 453 cm^{-1} related to O-Si-O bending vibration gradually disappear with decreasing the Si content[25, 26]. As shown in Fig.4(b), there are no obvious changes in the FTIR spectra of G1 and GC1 sample, indicating that crystallization process has little impact on Si-O network in G1 sample because crystallization only occur in fluoride phase. However, the band at around 1045 cm^{-1} was decreased and the band at around 615 cm^{-1} was enhanced after the heat-treatment of G5 sample, suggesting the change of Ge- bond in Ge-rich glass during heat-treatment process. It may be because of the ion diffusion of the nucleation of the volume crystallization. As shown in Fig.4(c), similar vibration changes of Si-O bond and Ge-O bond can be found in Raman spectra. Moreover, for glass ceramics containing $NaYF_4$ nanocrystals such as GC1, we can find Raman peaks at around 280 cm^{-1} due to the vibration of Na-F and Y-F bonds in $NaYF_4$ NCs, and the peak intensity was positively associated with NCs content. It can not find in Si-rich glasses such as G1 and in Ge-rich glasses and glass ceramics such as G5 and GC5, as presented in Fig.4(d). Besides, the intensity of GC1 ranging from 100 to 800 cm^{-1} in the Raman spectra is higher than that of G1 which can be attributed to the higher polarization of glass ceramic material. And the intensity of the GC5 is slightly higher than that of the G5 which may be caused by the nucleation of glass during the heat-treatment process.

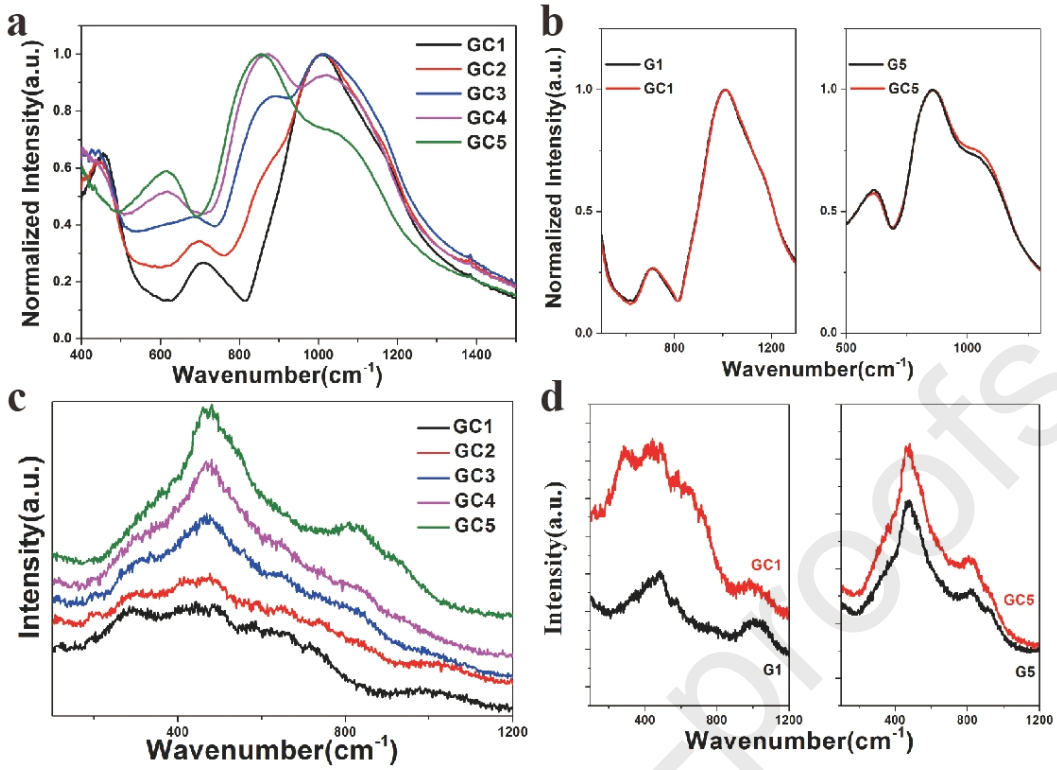

Fig.4 FTIR absorption spectra (a) and Raman spectra (c) of oxyfluoride glass ceramics with different Si/Ge ratio; comparsions of G1 and GC1 as well as G5 and GC5 in FTIR absorption spectra (b) and Raman spectra(d).

The decreased ability of $NaYF_4$ crystallization in oxyfluoride germanosilicate glass with more Ge content can be explained as follows.

The immiscibility of oxyfluoride silicate glass is higher than that of the oxyfluoride germanate glass from crystal chemistry aspect, which is linked to the different field strength or electroscopic bond strength of the central cation in polyhedral. The order of the cation field strength that can be determined by the ionic valence and the ion radius, is $Si^{4+}>Ge^{4+}>Al^{3+}>Y^{3+}>Na^{+}$. In previous investigation in SiO_2-Al_2O_3-BaF_2 glass ceramic, the forming of Si-O and Al-O bonds is prior than Ba-O and Most of the Ba^{2+} will coordinate to F^{-} with ionic bonds, and thus [SiO_4] composite the oxide network skeleton while the [AlO_xF_y] composite the phase interface of oxide phase and fluoride phase. However, in oxyfluoride germanate glass, the field strength of Ge^{4+} is only slightly higher than that of Al^{3+}, and therefore, the fluoride phase separation is more difficult. Multi structural units in germanate glass also indicates a stronger inclusiveness of oxyfluoride germanate glass.

The crystallization activation energy and temperature of oxide glass component containing more Ge is lower than that of oxide glass component containing more Si, possibly leading to a crystallization mutual perturbation between fluoride glass component and oxide glass component containing more Ge. Instead, there is a simultaneous crystallization of fluoride glass component and oxide glass component at a higher temperature.

Fluorine loss can occur in the glass preparation procedure[27], and it is likely that GeO_2-rich glasses might suffer from more significant loss of fluorine due to the lower

melting temperatures of GeO_2 compared with SiO_2, which limits the fluorine source of fluoride phase. It is noted that the NaF and YF_3 raw material have lower melting points than other fluoride component which can be crystallized in the oxyfluoride germanate glasses in a similar melting temperature, such as CaF_2 and LaF_3. Therefore, a new designed germanate glass composition with lower melting temperature may appear the oxide and fluoride phase separation phenomenon.

3.2 Absorption spectra and Judd-Ofelt parameters

The absorption spectra of glasses and glass ceramics with different Si/Ge ratio in the range of 300-1500 nm at room temperature were shown in Fig.5(a) and Fig.5(b), where the characteristic absorption bands of rare earth ions corresponding to the transitions starting from ground states (Ho^{3+}: $^5I_7$ level) to excited states are labeled. Here, the intensity of absorption spectra of glasses and glass ceramics is different, the former is for better illuminating the absorption peaks of rare earth ions while the later is for better showing the absorption cut-off wavelength. The saltation around 860nm in the absorption spectra were caused by the instrument error of switching detector. The strong absorption bands centered at 975 nm corresponding to the Yb^{3+} transition $^2F_{7/2}\rightarrow{}^2F_{5/2}$ indicate that Yb^{3+} ions can provide an efficient excitation channel when pumped by commercialized 980 nm laser diode. In addition, the characteristic absorption peaks of Ho^{3+} ions located at 1200nm, 642nm, 537nm, 484nm, 450nm, 417nm and 359nm were also observed, corresponding to the Ho^{3+} ions' transitions starting from the $^5I_8$ ground state to $^5I_6$, $^5F_5$, $^5F_4$+$^5S_2$, $^5F_3$, $^5F_1$+$^5G_6$, $^5G_5$ and $^5G_2$ excited states, respectively[6]. The Si/Ge ratio of oxyfluoride germanosilicate glasses have no influence on the shape and position of these absorption bands, and it was clearly because Ho^{3+} ions were protected by 4f electron shell and its energy levels are not vulnerable to surrounding glass host environment. There was no obvious variation of characteristic absorption bands with Si/Ge ratio of glass ceramics. The absorption cut-off wavelengths of glass ceramics were all shown a red shift compared with that of the corresponding glasses, which visually obscure the absorption bands of Ho^{3+} ions in glass ceramics. The red shift phenomenon was caused by the light scattering of NCs in glass. It was found that the shortest absorption cut-off wavelength in glass ceramic samples was that of the GCH2 sample, suggesting the weakest light scattering of GCH2 sample in all glass ceramic samples. The light scattering is affected by the density micro-changes of internal composition of glass. In the glass system, light scattering is mainly caused by the density difference between two different phases originating from the prevalent phenomenon of liquid-liquid phase separation in oxyfluoride glass. In addition, for GCs, the particle size and range of NCs dispersed in GCs have large impact on the light scattering intensity. The phase in oxyfluoride glass can be classified as glass forming phase that is mainly made up of network formers such as Si and Ge, and crystalline phase that is primarily composed of network modifiers[15]. Here we can infer that the density value of glass forming phase is lower than that of crystalline phase, since the density value of SiO_2 is lower than those of Na_2O, YF_3, YbF_3, HoF_3 and Al_2O_3. Appropriate substitution of GeO_2 with high density can increase the density of the glass forming phase and improve the

homogeneity of oxyfluoride glass. But further replacement of GeO_2 can cause the decreased fluoride phase separation and an excessive density of the glass forming phase and enlarge the density micro-changes inside glass, leading to a higher light scattering intensity in glass. This indicates that researchers can obtain oxyfluoride glass ceramics with low light scattering by minimizing the density difference between two different phases via glass composition control. As indicated by XRD patterns, the GCH5 is basically amorphous but it presents the highest scattering here, the heat-treatment may increase the microheterogeneity of glass structure as the Si0Ge55 635 sample has been softened and deformed, and nucleation of volume crystallization may have already happened as indicated by Raman spectra. Moreover, in oxyfluoride GC fibers, the influence of scattering loss on the infrared spectrum was smaller than that on the visible spectrum, suggesting the prepared GCs with low light scattering are more likely to acquire efficient GC fiber infrared lasers and amplifiers[28].

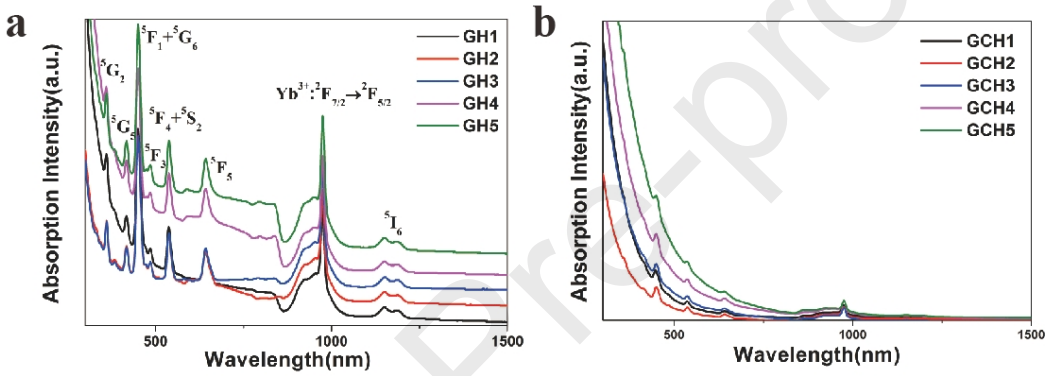

Fig.5 Absorption spectra of Yb/Ho codoped oxyfluoride glasses (a) and glass ceramics (b) with different Si/Ge ratio

The densities and J-O parameters of oxyfluoride glasses and glass ceramics with different Si/Ge ratio are shown in Table1. Obviously, with increased Ge content in samples, the density is gradually increased. The J-O parameters Ω_λ (λ=2,4,6) are determined via the least-squares methods, by minimizing the sums of the squares of the difference between theoretical and experimental dipole strengths according to measured absorption spectra and Judd-Ofelt theory[29, 30] The experimental dipole strengths of Ho^{3+} ions' transitions are extracted from the absorption spectra. The refractive index of glass samples and reduced matrix elements for transitions, which are insensitive to the host environment and obtained from the literature, are necessary for the calculation of theoretical dipole strengths of the electric dipole transitions. One can find that Ω_2 was increased with Ge content in oxyfluoride glasses. As discussed in structural analysis, heavy metal ion Ge^{4+} has a strong attraction to F^-, which can result in decreased Ho-F bonds and increased Ho-O bonds. Therefore, the ligand environment of Ho^{3+} ions becomes more asymmetrical and covalent. However, the Ω_2 variation behaviour becomes complex because of crystallization. Although $NaYF_4$ nanocrystals were not precipitated in GCH5 as shown in the XRD results, the Ω_2 changed largely from GH5 to GCH5, which suggests F^- ions may move to the vicinity of Ho^{3+} ions during the heat-treatment process.

Table1 Densities and Judd-Ofelt parameters of Yb/Ho codoped oxyfluoride glasses and glass ceramics with different Si/Ge ratio

Glass samples	ρ(g/cm^3)	Ω_2(×10^{-20}cm^2)	Ω_4(×10^{-20}cm^2)	Ω_6(×10^{-20}cm^2)
GH1	2.794	3.32	3.40	1.23
GH2	2.874	3.46	3.96	1.16
GH3	3.058	3.56	3.64	1.29
GH4	3.206	3.65	3.77	1.35
GH5	3.389	3.70	3.56	1.31
GCH1	2.845	1.95	1.99	0.77
GCH2	2.959	2.8	3.14	0.89
GCH3	3.099	2.14	2.88	0.81
GCH4	3.254	1.96	2.2	1.05
GCH5	3.401	1.1	1.22	0.96

3.3 VIS-NIR emission properties

Three visible upconversion emission bands could be observed in SiO_2-rich glass ceramics (Fig. 6(a)) and GeO_2-rich glass ceramics (Fig. 6(b)), whose peaks are located at 546 nm, 659 nm and 752 nm corresponding to the Ho^{3+}: $^5S_2$, $^5F_4 \rightarrow {}^5I_8$, $^5S_2 \rightarrow {}^5I_8$ and $^5S_2$, $^5F_4 \rightarrow {}^5I_7$ transitions. The 1.2 μm emission spectra of SiO_2-rich glass ceramics and GeO_2-rich glass ceramics are illustrated in Fig. 6(c) and Fig. 6(d), respectively. For SiO_2-rich glass and glass ceramics, the upconversion emissions and NIR emission are both enhanced with the heat-treatment temperature. This is because more rare earth ions located at fluoride nanocrystals with low phonon energy, in which the multi-phonon assisted non-radiative decay rates is significantly reduced so that the radiative emission is enhanced[4, 22, 23]. For GeO_2-rich glass and glass ceramics, the upconversion emission and NIR emission of glass ceramics are stronger than those of the precursor glass, but not shown a positive correlation with the heat-treatment temperature because there is no similar fluoride nanocrystallization.

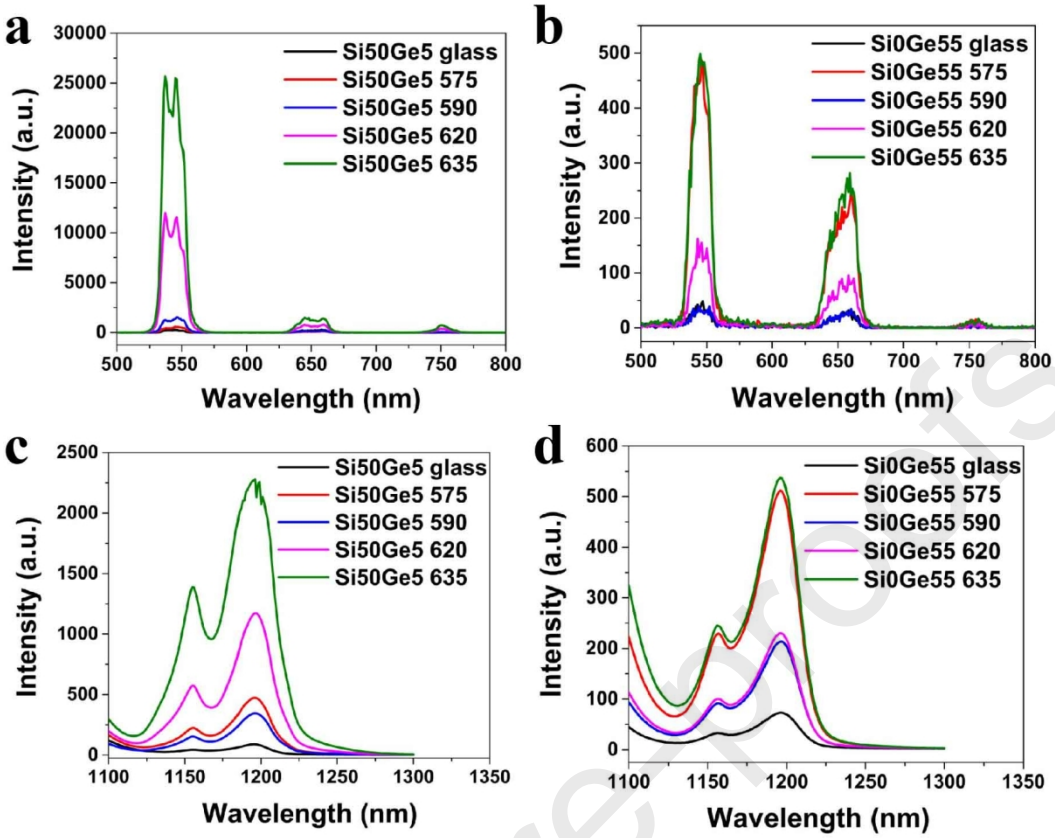

Fig. 6 Upconversion visible emission spectra of Yb/Ho codoped Si50Ge5 glass ceramics (a) and Si0Ge55 glass ceramics (b) with different heat-treatment temperatures pumped by 980nm LD; Near-infrared emission spectra of Yb/Ho codoped Si50Ge5 glass ceramics (c) and Si0Ge55 glass ceramics (d) with different heat-treatment temperatures pumped by 980nm LD.

As shown in Figure. 7(a) and 7(b), the fluorescent decay of Ho^{3+}: $^5I_6$ energy level monitored by 1190nm NIR emission show a great difference between the glasses and glass ceramics with different Si/Ge ratio. The inset presents the average fluorescent lifetime which is calculated by double-exponential non-linear fitting with a ±0.001 ms error. With the GeO_2 content increases, the Ho^{3+} lifetime in glasses presents a sightly decreasing trend. Interestingly, the Ho^{3+} lifetime in glass ceramics shows a drastic variation. A fast decay and a subsequent slow decay were obviously observed for the Si20Ge35 635 sample and the Si10Ge45 635 sample, which can be attributed to the Ho^{3+} ions located at glass matrix with high non-radiative decay rates and fluoride nanocrystals with low non-radiative decay rates.

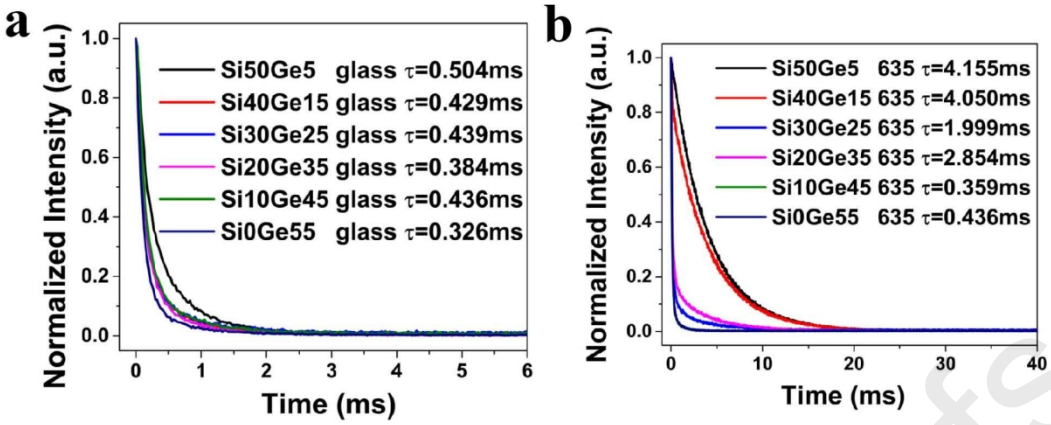

Fig.7 Decay curves of 1190nm in Yb/Ho codoped Si50Ge5 glass ceramics (a) and Si0Ge55 glass ceramics (b) with different Si/Ge ratio pumped by 980nm LD.

3.4 Mid-infrared emission properties

In order to study the influence of Si/Ge ratio on the 2 μm and 2.9μm emissions of prepared oxyfluoride glasses and glass ceramics, we measured their fluorescent spectra ranging from 1800nm to 2200nm and 2700nm to 3100nm under 980nm LD pumping as shown in Fig.8.

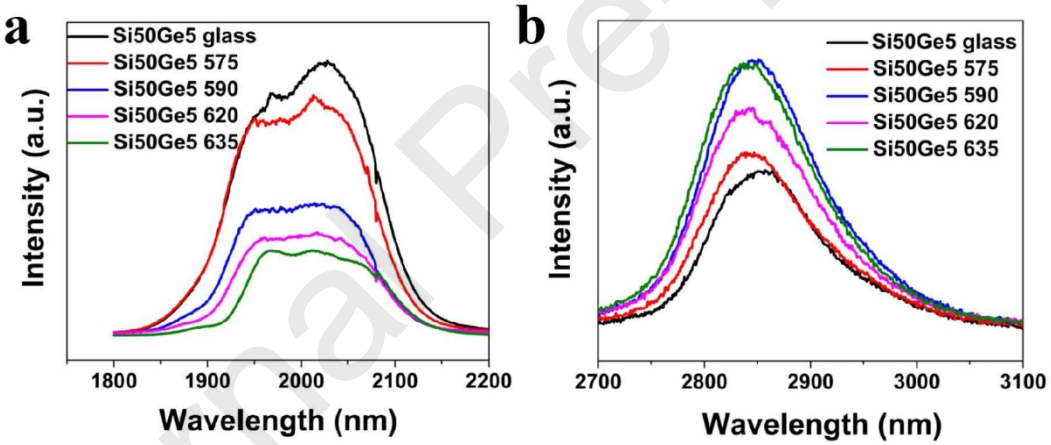

Fig.8 2μm emission spectra (a) and 3μm emission spectra (b) of Yb/Ho codoped Si50Ge5 glass ceramics with different heat-treatment temperature pumped by 980nm

As shown in Fig.9(a), emissions centered at 2.05μm were observed in all glasses with different Si/Ge ratio. The central position and shape of emission peaks are basically the same, but the intensity of emission peak gradually decrease with the Ge content in glass increases. The inset of Fig.9(a) indicates the simplified energy levels diagram and energy transfer process between Yb^{3+} and Ho^{3+} ions. With the increasement of Ge content in oxyfluoride glass, the state densities of phonons with high energy (Si-O-Si bond, as revealed by FTIR spectra) were decreased, leading to a decreased non-radiative decay rate between Ho^{3+}: $^5I_6$ and $^5I_7$ levels. So the population in Ho^{3+}:$^5I_7$ level was reduced and corresponding 2μm emission was decreased gradually. However, there was a different trend of 2μm emission intensities for GCs, as shown in Fig.9(b). The 2μm emission intensity was remarkably enhanced from GCH1 to GCH2, and then gradually dropped with the Ge content in GCs increases.

This was possibly because the concentration of Ho^{3+} ions located in NCs reaches a critical point between GCH1 and GCH2, since the 2μm emission may be enhanced or reduced according to the doping concentration of Yb^{3+}/Ho^{3+} ions[31].

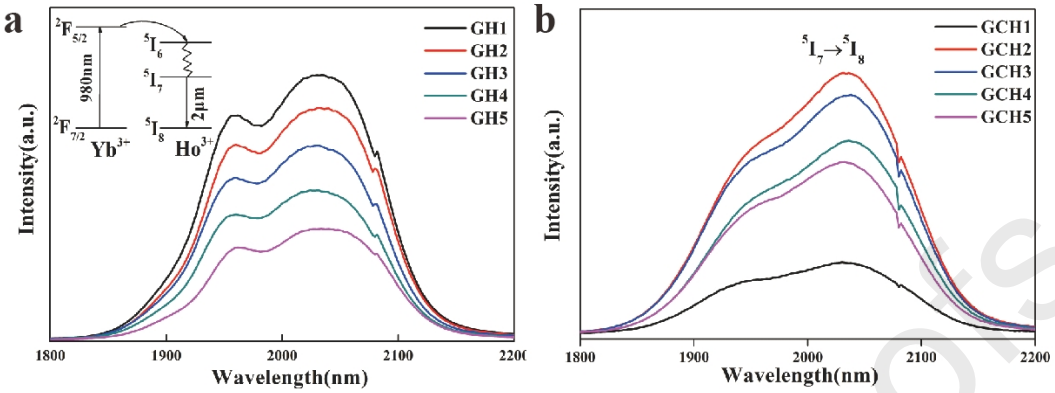

Fig.9 2μm emission spectra of Yb/Ho codoped oxyfluoride glasses (a) and glass ceramics (b) with different Si/Ge ratio pumped by 980nm LD

As shown in Fig.10(a), weak emissions centered at 2.9μm can be found in all glasses with different Si/Ge ratio. The weak emissions in oxyfluoride glasses were due to the phonon energy of glasses were relatively large, while the energy gap between Ho^{3+}: $^5I_6$ and $^5I_7$ levels was comparatively small. Accordingly, the ions at Ho^{3+}: $^5I_6$ level were easily non-radiative decay to Ho^{3+}: $^5I_7$ level, and the corresponding 2.9μm emissions were very weak. By contrast, strong 2.9μm emissions were observed in oxyfluoride glass ceramics, and its fluorescent intensity decreased when the Ge content increased, as shown in Fig.10(b). With the increasement of Ge content in oxyfluoride glass, the number of precipitated $NaYF_4$ NCs was decreased as revealed by XRD patterns. As a result, the number of Ho^{3+} ions located at low phonon energy environment was reduced so that the corresponding 2.9μm emission was decreased gradually.

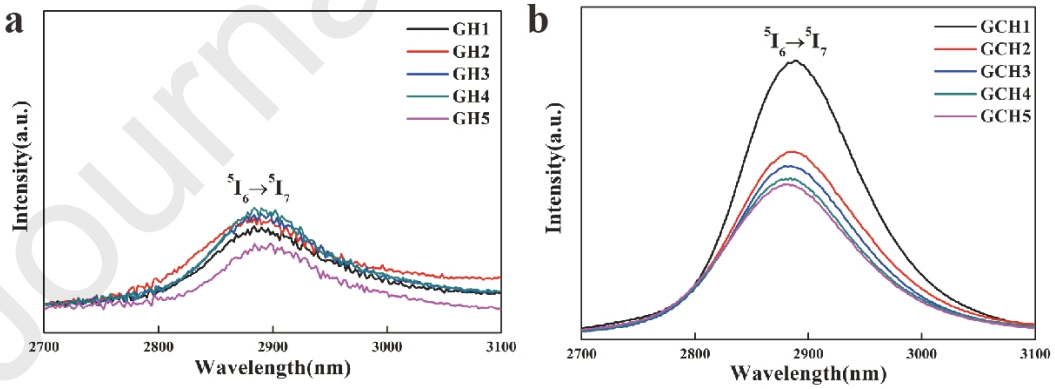

Fig.10 3μm emission spectra of Yb/Ho codoped oxyfluoride glasses (a) and glass ceramics (b) with different Si/Ge ratio pumped by 980nm LD

To further evaluate the mid-infrared luminescent properties of prepared GCs and its potential as mid-infrared laser materials, based on the Fuchtbauer-Ladenburg formula (1) and the McCumber relationship formula (2)[32], the absorption and emission cross sections and gain spectrum of GCH2 sample that has the weakest

scattering loss were calculated and presented in Fig.11(a).

$$\sigma_{em}(\lambda) = \frac{\lambda^5 A_{rad}}{8\pi c n^2} \frac{I(\lambda)}{\int \lambda I(\lambda) d(\lambda)} \tag{1}$$

$$\sigma_e = \sigma_a(\lambda) \exp\left[(\varepsilon - h\nu) / kT\right] \tag{2}$$

The calculation results showed that the peak absorption cross section reached 9.93×10^{-21}cm^2 at 2880 nm, while the peak emission cross section reached 11.18×10^{-21}cm^2 at 2888 nm which is higher than that of oxyfluoride silicate GC(6.0×10^{-21}cm^2)[4]. Obviously, it can be attributed to the higher density of oxyfluoride germanosilicate GC, as there is a positive correlation between density and absorption and emission cross sections. According to formula(3):

$$G(\lambda, P) = N \times \left[P \times \sigma_{em} - (1 - P) \times \sigma_{abs}\right] \tag{3}$$

where N is the Ho^{3+} ions concentration in GCH2 sample and P is the inversion factor given by the ratio of $^5I_6$ and $^5I_7$ energy level. The gain coefficient spectrum of the GCH2 sample at 2.9μm is shown in Fig.11(b). Its maximum gain coefficient is 1.387 cm^{-1}, and central wavelength is 2888nm. So an inversion of population between the $^5I_6$ level and $^5I_7$ level can be achieved efficiently, and the gain in resonator can effectively overcomes the losses, generating robust 2.9μm laser beam.

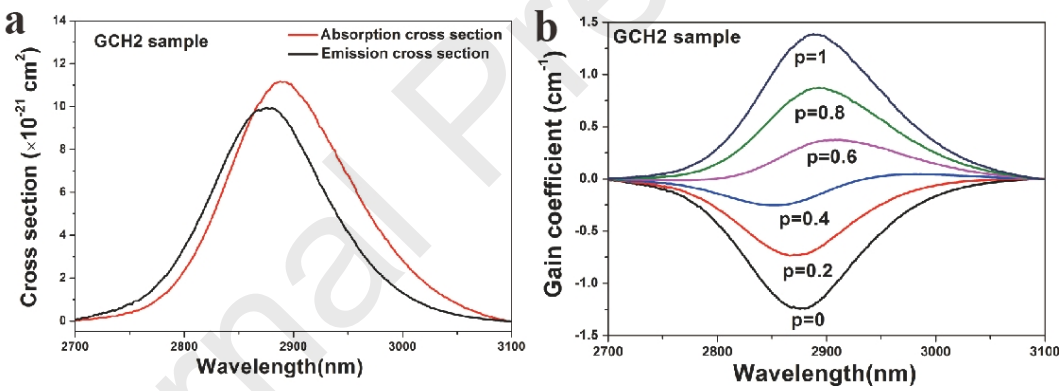

Fig.11 Absorption and emission cross section (a) and gain coefficient spectra (b) of GCH2 sample

4. Conclusion

Oxyfluoride germanosilicate glasses and glass ceramics with different Si/Ge ratio were prepared by the conventional high-temperature melt-quenching technique. The $NaYF_4$ nanocrystals crystallization ability of oxyfluoride glass was decreased with the increase in Ge content because of the weakened oxide and fluoride phase separation in GeO_2-rich glass. The weakened phase separation is explained from three parts: the immiscibility of oxyfluoride glass from the crystal chemistry aspect, the effect of oxide glass phase, and the fluorine loss in the glass melting procedure. The results of absorption spectra indicate that oxyfluoride glass ceramics with low light scattering can be obtained by minimizing the density difference between two different phases via glass composition control. Upconversion and down-conversion emission spectra

together with Ho^{3+}: $^5I_6$ energy level fluorescent decay curves have been discussed for SiO_2-rich glass ceramics and GeO_2-rich glass ceramics, in which the fluoride crystallization induced the decrease of multi-phonon non-radiative decay rates plays the main role in the energy transfer processes. The influence of Si/Ge ratio on 2μm and 2.9μm fluorescent emissions in glasses and GCs were discussed. The emissions of glasses mainly related to the state densities of phonons with high energy, while the emissions of GCs were largely affected by the concentration of Ho^{3+} ions located in NCs resulting from varying crystallization behaviour in GCs. The low light scattering, high peak emission cross section($11.18\times10^{-21}cm^2$) and maximum gain coefficient (1.387 cm^{-1}) at 2888 nm of GCH2 sample show its potential application in the development of new 3μm laser devices based on transparent oxyfluoride glass ceramic materials.

Acknowlegement

The authors are thankful to the Zhejiang Provincial Natural Science Foundation of China (LZ21F050002),the National Natural Science Foundation of China (nos.61775205, 51472225, 61405182 and 61605192) and Science and Technology Innovation Platform and Talent Plan of Zhejiang (2017R52037), and National Key Research and Development Project of China(2018YFE0207700).

References

1. N. P. Barnes, B. M. Walsh, D. J. Reichle and R. J. DeYoung, *Optical Materials*, 2009, **31**, 1061-1064.
2. S. D. Jackson, *Nature photonics*, 2012, **6**, 423-431.
3. P. Zhou, X. Wang, Y. Ma, H. Lü and Z. Liu, *Laser Physics*, 2012, **22**, 1744-1751.
4. Q. Liu, Y. Tian, C. Wang, F. Huang, X. Jing, J. Zhang, X. Zhang and S. Xu, *Physical Chemistry Chemical Physics*, 2017, **19**, 29833-29839.
5. W. Q. Cao, F. F. Huang, R. G. Ye, M. Z. Cai, R. S. Lei, J. J. Zhang, S. Q. Xu and X. H. Zhang, *Journal of Alloys and Compounds*, 2018, **746**, 540-548.
6. Y. Tian, L. Y. Zhang, S. Y. Feng, R. R. Xu, L. L. Hu and J. J. Zhang, *Optical Materials*, 2010, **32**, 1508-1513.
7. V. Lupei, *Reference Module in Materials Science and Materials Engineering*, 2016, 4416-4423.

8. A. Ikesue and Y. L. Aung, *Nature Photonics*, 2008, **2**, 721.

9. A. Jha, B. Richards, G. Jose, T. Teddy-Fernandez, P. Joshi, X. Jiang and J. Lousteau, *Progress in Materials Science*, 2012, **57**, 1426-1491.

10. W. C. Wang, B. Zhou, S. H. Xu, Z. M. Yang and Q. Y. Zhang, *Progress In Materials Science*, 2019, **101**, 90-171.

11. E. D. Zanotto, *International Journal of Applied Glass Science*, 2013, **4**, 105-116.

12. A. de Pablos-Martín, A. Durán and M. J. Pascual, *International Materials Reviews*, 2012, **57**, 165-186.

13. J. Zhao, X. Zheng, E. P. Schartner, P. Ionescu, R. Zhang, T.-L. Nguyen, D. Jin and H. Ebendorff-Heidepriem, *Advanced Optical Materials*, 2016, **4**, 1507-1517.

14. P. P. Fedorov, A. A. Luginina and A. I. Popov, *Journal of Fluorine Chemistry*, 2015, **172**, 22-50.

15. X. Liu, J. Zhou, S. Zhou, Y. Yue and J. Qiu, *Progress in Materials Science*, 2018, **97**, 38-96.

16. O. Majerus, L. Cormier, D. R. Neuville, L. Galoisy and G. Calas, *Journal Of Non-Crystalline Solids*, 2008, **354**, 2004-2009.

17. G. S. Henderson, D. R. Neuville, B. Cochain and L. Cormier, *Journal Of Non-Crystalline Solids*, 2009, **355**, 468-474.

18. X. Y. Li, D. Q. Chen, F. Huang, G. C. Chang, J. J. Zhao, X. S. Qiao, X. H. Xu, J. C. Du and M. Yin, *Laser & Photonics Reviews*, 2018, **12**, 8.

19. J. Ren, X. Lu, C. Lin, and R. K. Jain, Optics Express, 2020, 28(15), 21522-21548.

20. J. Zhao, X. Xu, X. Chen, Q. Xu, Z. Luo, X. Qiao, J. Du, X. Fan and G. Qian, Journal

of the European Ceramic Society, 2019, 39, 5018-5029.

21. S. Wang, J. Lina, Y. He, J. Chen, C. Yang, F. Huang, D. Chen, Chemical Engineering Journal 2020, 394, 124889.

22. T. Ouyang, S. Kang, Z. Zhang, D. Yang, X. Huang, Q. Pan, J. Gan, J. Qiu and G. Dong, Adv.OpticalMater.2019, 7, 1900197.

23. S. Kang, Z. Fang, X. Huang, Z. Chen, D. Yang, X. Xiao, J. Qiud and G.Dong, Journal of the Material Chemistry C, 2017, 5, 4549.

24. O. Majérus, L. Cormier, D. R. Neuville, L. Galoisy and G. Calas, *Journal of Non-Crystalline Solids*, 2008, **354**, 2004-2009.

25. M. Kasprzyk, M. Sroda and M. Szumera, *J. Therm. Anal. Calorim.*, 2017, **130**, 207-220.

26. J. Partyka and M. Lesniak, *Spectroc. Acta Pt. A-Molec. Biomolec. Spectr.*, 2016, **152**, 82-91.

27. L.A. Bueno, Y. Messaddeq, F.A. Dias Filho and S.J.L. Ribeiro, Journal of Non-Crystalline Solids, 2005, 351, 3804–3808.

28. B. N. Samson, P. A. Tick and N. F. Borrelli, *Optics letters*, 2001, **26**, 145-147.

29. B. R. Judd, *Phys. Rev.*, 1962, **127**, 750-761.

30. G. S. Ofelt, *J. Chem. Phys.*, 1962, **37**, 511-520.

31. G. Dominiak-Dzik, R. Lisiecki, W. Ryba-Romanowski and L. Krajczyk, *Journal of Alloys and Compounds*, 2012, **511**, 189-194.

32. D. E. McCumber, *Phys Rev.*, 1964, **134**, 299-306.

Highlights

The structure and mid-infrared luminescence in glass ceramics was investigated.

Oxyfluoride germanosilicate glass ceramics with varied Si/Ge ratio are prepared.

The influence of Si/Ge ratio on mid-infrared luminescence of samples were discussed.

Prepared glass ceramics possesses high emission cross section and gain coefficient.